Paper No. 141

A two-stage nucleation model with incubation effect for hydride precipitation in zirconium alloys

Kolesnik M.[1], Stuckert J.[1], Groβe M.[1]

[1]Institute of Applied Materials – Applied Materials Physics (IAM-AWP), Karlsruhe Institute of Technology, Karlsruhe, Germany

ABSTRACT

Hydrogen accumulates in zirconium alloy cladding tubes during reactor operation as a by-product of waterside corrosion. When its concentration exceeds the solid solubility (TSS), plate-like hydrides precipitate, which may lead to embrittlement. The severity of embrittlement depends on hydrogen concentration and hydride morphology, including orientation, characteristic length, and connectivity of the hydride network. While hydrogen uptake is mainly governed by alloy composition and operating conditions, hydride morphology is strongly influenced by the post-operation thermal and mechanical history. Thermomechanical cycles during handling and storage can cause repeated dissolution and reprecipitation, promoting long, radially oriented hydrides that facilitate brittle crack propagation. Consequently, hydride-induced embrittlement becomes critical during handling and dry storage of spent nuclear fuel. Accurate prediction of hydride morphology requires a proper description of nucleation kinetics. In our previous approach, nucleation was modeled using classical theory; however, validation against recent experimental data showed excessive sensitivity to uncertainties in hydrogen concentration and solubility under certain thermal conditions. To overcome this limitation, a two-stage kinetic model with a finite incubation period has been developed. This concept is based on the formation of metastable precursor phases preceding the stable δ-hydride. The incubation period represents the time needed for hydrogen accumulation and local lattice rearrangement prior to stable nucleus formation. The present work introduces this model and demonstrates its effect on predicted hydride precipitation behavior.

Keywords: hydride embrittlement, zirconium alloys, hydride morphology, spent nuclear fuel, dry storage

1. INTRODUCTION

Dry storage is the primary technology for the long-term interim storage of spent nuclear fuel. Ensuring sufficient ductility of fuel cladding is a key safety requirement during storage, handling, and transport. However, thermomechanical conditions during dry storage may activate degradation mechanisms that compromise the mechanical integrity of zirconium alloy cladding, among which hydrogen-induced embrittlement is particularly critical.

Hydrogen accumulates in the cladding during reactor operation as a by-product of waterside corrosion [1], [2]. The resulting embrittlement is governed not only by the total hydrogen content but also by hydride morphology, which can promote preferential pathways for brittle crack propagation [3]. In turn, hydride morphology is controlled by the thermomechanical conditions governing nucleation and growth [2], [3]. At low applied stresses, hydride orientation is primarily determined by the crystallographic texture of the alloy [4], whereas above a critical stress threshold, hydrides preferentially orient perpendicular to the tensile stress direction [5].

Several hydride phases with different stoichiometries and crystal structures have been observed experimentally in zirconium, including HCP ζ-Zr_2H [6], FCT γ-ZrH ($c > a$) [7], FCC δ-$ZrH_{1.6}$ [8] and

FCT ε-ZrH_2 ($c < a$) [9]. Under conditions relevant to fuel operation and handling, the δ-phase is most commonly observed and considered stable [1]. The stability of the ζ- and γ-phases remains a subject of debate; in [10], they are considered metastable phases that may act as precursors to the stable δ-phase. First-principles calculations predict the existence of an even larger number of intermediate phases [11], [12], [13], supporting the hypothesis that the metal-to-hydride phase transformation may proceed through a sequence of metastable states. This phase transformation is accompanied by significant volumetric expansion, leading to dislocation emission into the metal matrix [14].

The growth of nano- and micro-scale single-crystal hydrides is limited by dislocation emission [15] and constrained by the grain size. Further growth proceeds via the nucleation of new nano-scale hydrides, predominantly at grain boundaries and in the vicinity of existing ones [16], [17]. Such agglomerations of nano- and micro-scale hydrides form ordered plate-like ("corn-flake") structures [18], with characteristic sizes ranging from tens to hundreds of micrometers. The nucleation rate of these macroscale hydrides is a strongly nonlinear function of hydrogen supersaturation: once a critical threshold is exceeded, rapid precipitation occurs, which accelerates supersaturation relaxation due to the increasing number of sinks. Consequently, the volumetric hydride density must be described within a coupled framework involving diffusion, supersaturation relaxation, and nucleation.

A comprehensive description of hydride morphology therefore requires quantitative parameters such as orientation of hydrides, mean hydride length, and volumetric hydride density. Corresponding predictive models must solve a coupled problem of hydrogen transport, orientation-dependent precipitation, and nucleation rate of new hydrides.

2. PROBLEM STATEMENT

A physically based model capable of predicting hydride orientation, mean length, and hydride density was previously developed [19], where the nucleation process is described within the framework of classical heterogeneous nucleation theory (CNT). However, limitations of this model became evident when applied to recent experimental results from the SPIZWURZ campaign conducted at KIT [20], [21]. In the SPIZWURZ experiments, hydrogen-charged cladding tubes were subjected to thermal cycling under constant internal gas pressure. Model predictions for hydride mean length and length density exhibited an excessive and physically unrealistic sensitivity to the assumed initial hydrogen concentration.

A representative example is rod 8 at an elevation of 520 mm, manufactured from Zircaloy-4, with a measured hydrogen concentration of 127 ppm (Table A2 in [21]). This concentration corresponds to the condition of complete hydride dissolution at the maximum test temperature of 400 °C. When the initial hydrogen concentration is varied within the uncertainty range of 127 ± 15 ppm, the calculated mean hydride length spans from 38 to 1600 μm, while the hydride density ranges from 10 to 450 mm^{-2}. In contrast, the experimentally measured values are 36.2 μm and 346 mm^{-2}, respectively (Fig. 1).

The origin of this excessive sensitivity can be traced to the strong dependence of the nucleation process on the cooling rate during the nucleation stage. The initial hydrogen concentration determines the precipitation temperature and, consequently, the time at which nucleation is initiated along the thermal history. In the model, nucleation occurs over a short time scale of approximately 5–60 minutes, which is negligible compared to the total duration of dry storage and of the SPIZWURZ simulation experiment (~250 days) for which the hydride morphology and orientation is available. As a result, nucleation effectively reduces to a point event on the temperature history, after which precipitation proceeds solely through the growth of already formed hydrides, without further nucleation. This indicates that the classical formulation effectively treats nucleation as a very fast (almost instantaneous on the scale of the SPIZWURZ experiment) event governed by local conditions, without accounting for the temporal persistence of the driving force.

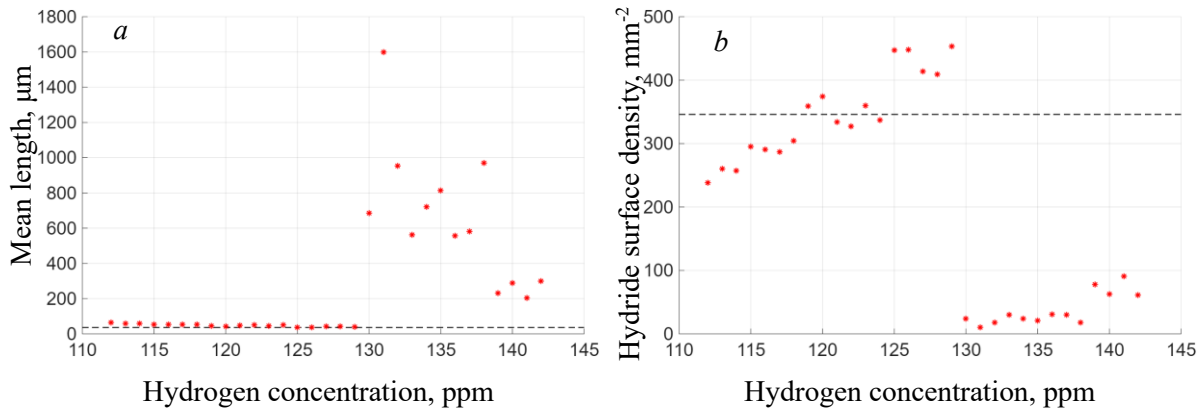


Figure 1. Simulation results with the initial version of the model based on the CNT; markers – simulation results; dotted line – experimental results

The temperature evolution in the SPIZWURZ experiment for the rod 8 selected as a representative example is shown in Fig. 2(*a*). It is characterized by a step-wise cooling regime, with temperature drops of approximately 15 °C, superimposed with slow, non-monotonic fluctuations of a few degrees and a characteristic period of about 24 hours (Fig. 2(*b*)). For the measured hydrogen concentration of 127 ppm, the nucleation temperature is 281.8 °C. When the hydrogen concentration is varied within the uncertainty range of 127 ± 15 ppm, the corresponding nucleation temperature shifts to the range of 271.2–291.6 °C, as indicated by the red markers in Fig. 2(*b*). As a result, nucleation is triggered under substantially different thermal conditions. In particular, the local cooling rates at the nucleation points differ by several orders of magnitude. This leads to pronounced variations in the volume density of nucleated hydrides, which in turn governs the predicted mean hydride length and surface density. Therefore, an improved nucleation model should significantly reduce sensitivity to instantaneous thermal conditions and short-time temperature fluctuations.

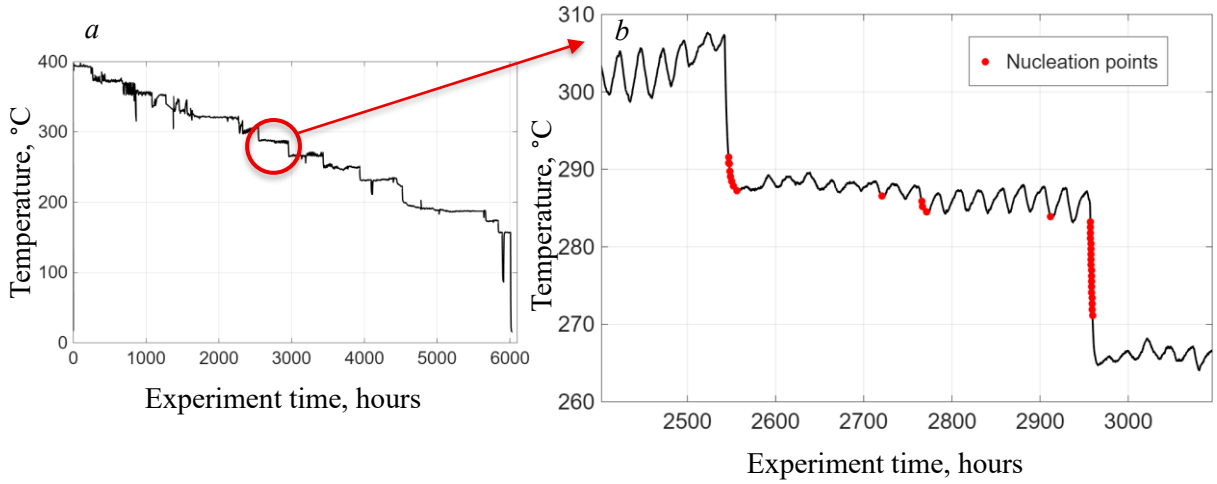


Figure 2. Temperature scenario (*a*) and points where nucleation starts when varying the hydrogen concetnration within its uncertainty (*b*)

3. NEW MODEL DESCRIPTION

3.1. Original model framework (unchanged components)

The proposed model builds upon the existing framework described in detail in [19]. The present extension is limited to the modification of the hydride nucleation sub-model, while all other components of the model are retained in their original form.

The kinetics of hydrogen in solid solution C_s is described in terms of supersaturation relaxation with a characteristic time, τ_0, as introduced in [19], [22]:

$$\frac{\mathrm{d}C_s}{\mathrm{d}t} - \frac{1}{\tau_0}\left(C_s - C_e\right) = 0 \tag{1}$$

where C_e – equilibrium solubility, which is different for precipitation (TSSP) and dissolution (TSSD). The characteristic time is determined as $\tau_0 = \Delta/\alpha^2 D_{\mathrm{H}}$, where Δ – mean distance between hydrides, α – geometry factor, D_{H} – diffusion coefficient of hydrogen in zirconium.

The cumulative fraction of hydrogen in radially oriented hydrides θ evolves during precipitation according to [19], [22]

$$\frac{\mathrm{d}\theta}{\mathrm{d}t} = -\frac{f_r - \theta}{C_{tot} - C_s} \cdot \frac{\mathrm{d}C_s}{\mathrm{d}t} \tag{2}$$

Here, C_{tot} is the total hydrogen concentration in the material, and f_r is the instantaneous fraction of hydrogen precipitating as radially oriented hydrides at the current time step. This fraction is assumed to be a function of the tangential stress, σ, and temperature, T [19], [22]:

$$f_r = \frac{1}{1 + f_0 \exp\left(-\dfrac{\sigma \cdot \Delta\Omega}{kT}\right)} \tag{3}$$

where f_0 and $\Delta\Omega$ are model parameters.

3.2. Two-step nucleation model

One of the simplifications adopted in model above, is to represent nucleation as the direct formation of stable δ-hydrides at lattice defects. However, this assumption neglects the experimentally and theoretically established multistage transformation sequence, in which stable hydrides form via intermediate metastable phases. In this context, multiphase models of hydride nucleation have previously been reported in the literature [23]. In the present formulation, the CNT framework is applied to the formation of metastable precursor states, while the subsequent transition to stable δ-hydrides is governed by transformation kinetics with a finite incubation time.

The physical basis of the present modeling approach is as follows. At the initial stage, hydrogen accumulates in localized regions near lattice defects, leading to the formation of hydrogen clusters. This is followed by a sequence of transformations involving metastable phases, accompanied by lattice rearrangement, volumetric expansion, and dislocation emission. These processes ultimately result in the formation of stable δ-hydrides.

The presence of metastable stages significantly affects nucleation kinetics. In particular, the formation of metastable phases is associated with a lower energy barrier compared to direct δ-phase nucleation, due to reduced interfacial energy and more efficient strain accommodation within the matrix.

To account for this multistage transformation, an additional state variable is introduced - the volumetric density of metastable nuclei, N_{ms}. The evolution of this variable governs the accumulation of

intermediate states and their conversion into stable hydrides. The nucleation frequency is determined by the Gibbs free energy change associated with nucleation, ΔG_n:

$$\Delta G_n = V_n\left(g_{mech} - x\frac{kT}{v_H}\cdot\log\left(C_s/C_e\right)\right) + S_n\gamma_n - S_{cs}\gamma_{gr} \tag{4}$$

where V_n, S_n – volume and surface area of the nucleus, x – stoichiometry of the hydride ($x = 1.6$ for δ-phase $ZrH_{1.6}$), v_H – atomic volume of hydrogen in the hydride phase, γ_n – interphase surface energy, γ_{gr} – grain energy in the nucleation area (the defect energy disappears after the nucleus has nucleated), S_{cs} – the area of the grain boundary covers the nucleus, which is equal to its cross-section, g_{mech} - mechanical energy change per unit volume.

The surface energy of nucleus, γ_n, depends on the phase and typically varies in the range of 0.035 – 0.2 J/m^2 [23]. The grain boundary energy, γ_{gr}, depends on the misorientation of the neighboring grains and can be considered a random variable of the same order of magnitude, i.e. up to 0.1 J/m^2. The nucleus-matrix interfacial area, S_n, and the contact area with the grain boundary, S_{cs}, both scale with the square of the nucleus radius and are related through geometric factor (S_n>S_{cs}). Therefore, to reduce the number of model parameters, the combined interfacial energy term is approximated as $S_n\gamma_n - S_{cs}\gamma_{gr} \approx S_n\gamma'$, where γ' is an effective surface energy associated with hydride nucleation at a given grain boundary. This parameter reflects the variability in grain boundary character and is assumed to follow a lognormal distribution with a maximum probability density around 0.03 J/m^2. The nucleation frequency $J_{n,ms}$ of the metastable hydrides is then calculated according to the CNT:

$$J_{n,ms} = \int_{\gamma'_{\min}}^{\gamma'_{\max}} n_{\max}\left(\gamma'\right)\cdot Z\left(\gamma'\right)\cdot j^*\left(\gamma'\right)\cdot\exp\left(-\Delta G_n^*\left(\gamma'\right)/kT\right)\cdot\mathrm{d}\gamma' \tag{5}$$

where $n_{\max}(\gamma')$ – the distribution of nucleation sites as a function of the effective surface energy, $Z = [\Delta G_n(r^*)/(3\pi kT\cdot(V^*/v_H)^2)]^{1/2}$ – Zeldovich factor, V^* – hydride volume, $j^* = 4\pi \mathrm{D_H} r^*\cdot(C_s - C_e)$ – the hydrogen sink the superscript "*" denotes the critical nucleus.

The volumetric density of metastable nuclei, N_{ms}, changes due to their formation, transformation into stable hydrides, and decomposition back into the solid solution:

$$\frac{\mathrm{d}N_{ms}}{\mathrm{d}t} = J_{n,ms} - J_{dec} - J_{tr} \tag{6}$$

here J_{tr} and J_{dec}, denote transformation of metastable into stable hydrides and their decomposition back into the solid solution, respectively. Transformation is active while the conditions for nucleation remain favorable and is described as $J_{tr} = N_{ms}/\tau_{inc}$, where τ_{inc} is the incubation time, described in the following section. If these conditions are no longer satisfied, transformation is suppressed and the metastable nuclei decompose according to $J_{dec} = N_{ms}/\tau_{dec}$, where τ_{dec} is the characteristic decomposition time.

3.3. Incubation time

Another simplification adopted in [19] is the direct use of the steady-state nucleation rate (Eq. (5)). In reality, however, the nucleation process is characterized by a finite time lag required for the nucleation rate to reach its steady-state value, commonly referred to as the incubation time [24]. The present formulation represents an effective incubation period governed by coupled diffusion and phase transformation processes.

In the present work, the incubation time is interpreted as the characteristic time required for the phase transformation leading to the formation of a stable hydride nucleus. This time scale reflects a sequence of coupled physical processes occurring at the microscale, including: (i) accumulation of hydrogen in the vicinity of lattice defects (diffusion-driven formation of Cottrell atmospheres); (ii) local lattice rearrangement governed by atomic jump frequencies; (iii) formation of metastable hydride phases and subsequent increase in hydrogen stoichiometry; and (iv) relaxation of the associated mechanical energy

through dislocation emission and plastic accommodation. Among these processes, the rate-limiting steps are associated with hydrogen transport, namely the formation of Cottrell atmospheres and the subsequent diffusive flux required to sustain phase transitions and stoichiometry evolution. It should be taken into account that the formation of hydrogen clusters is accompanied by a transient depletion of hydrogen in the surrounding solid solution and requires hydrogen redistribution over a length scale exceeding the size of the nucleus (here, the characteristic diffusion length is assumed to be on the order of the alloy grain size).

The incubation time governed by diffusion processes is estimated here as follows. The diffusive flux toward the nucleus can be approximated as $J = -D_{\mathrm{H}} \cdot \nabla C_{\mathrm{H}} \approx -D_{\mathrm{H}} \cdot (C_s - C_e)/L_{eff}$, where L_{eff} is the characteristic diffusion length (on the order of the grain size). The formation of a nucleus requires the accumulation of hydrogen atoms in an amount $N_{\mathrm{H}} \approx C_{hyd} \cdot r_{hyd}^3$, where C_{hyd} is the hydrogen concentration in the hydride and r_{hyd} is the radius of the hydride. Accordingly, the characteristic diffusion-controlled incubation time τ_{inc} can be estimated as:

$$\tau_{inc} \approx \frac{N_H}{SJ} \approx \frac{r_{hyd}^3 \cdot C_{hyd}}{r_{hyd}^2} \cdot \frac{L_{eff}}{D_H \left(C_s - C_e\right)} \approx \frac{r_{hyd} L_{eff}}{D_H} \cdot \frac{C_{hyd}}{C_s - C_e} \tag{7}$$

For nucleation to occur, it is necessary that the conditions favorable for nucleation be maintained continuously throughout the entire incubation period. Under these conditions, metastable nuclei rearrange into stable ones, which is described by the following system of equations:

$$\frac{\mathrm{d}N_{r,t}}{\mathrm{d}t} = f_{r,t} \frac{N_{ms}}{\tau_{inc}} \tag{8}$$

here $N_{r,t}$ are volumetric densities of radial and tangential hydrides, $f_{r,t}$ are instantaneous fractions of radial and tangential hydrides precipitating on the current time step, $f_t = 1 - f_r$. The estimated incubation time τ_{inc} yields a characteristic value on the order of minutes.

4. RESULTS AND DISCUSSION

The updated model is formulated as a system of five coupled differential equations describing hydride nucleation and growth processes. Specifically, Eqs. (1), (2), (5), and (7) are solved numerically (the latter providing two separate equations for radial and tangential hydrides). The set of independent kinetic variables includes: the hydrogen concentration in solid solution C_s, the cumulative fraction of hydrogen precipitated as radial hydrides θ, the volumetric density of metastable nuclei N_{ms}, and the volumetric densities of stable radial N_r and tangential N_t hydrides.

The predictive capability of the modified model was assessed by simulating the same thermal–mechanical scenario previously analyzed using the original model. The result is shown in Fig. 3 by analogy with Fig. 1. The introduction of the two-stage nucleation mechanism and incubation effects leads to a pronounced reduction in the sensitivity of the model to variations of cooling rate during nucleation in hydrogen content. In particular, the scatter of calculated mean hydride length is reduced to 28–96 μm, compared to 38–1600 μm obtained with the original model, while the corresponding experimental value is 36.2 μm. Similarly, the scatter of calculated hydride density is narrowed to 200–660 mm^{-2}, in contrast to 10–450 mm^{-2} for the original model, with the experimental reference value being 346 mm^{-2}. These results indicate that the updated model provides a substantially more realistic representation of hydride morphology evolution under the considered conditions.

The remaining scatter in the predicted quantities is considered acceptable, particularly in comparison with the previous model version. Nevertheless, it should be noted that the variability of the calculated results with respect to hydrogen content still exceeds the scatter observed in experimental data under similar conditions. For example, measurements performed at different axial positions of the specimen (where hydrogen concentration and temperature histories slightly varies) exhibit a narrower dispersion of hydride morphology [21]. This discrepancy suggests that further refinement of the model is required.

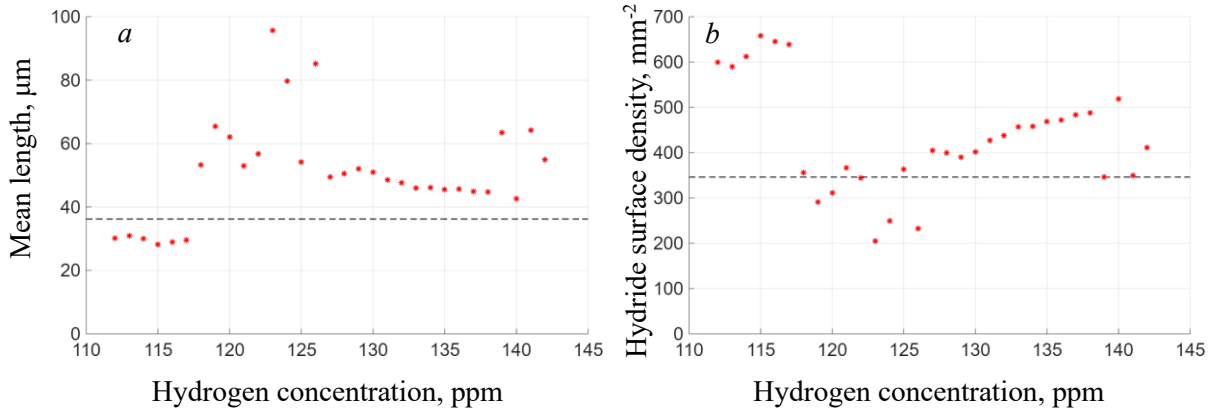


Figure 3. Simulation results with the updated version of the model based on the CNT; markers – simulation results; dotted line – experimental results

An additional comparison between the two models was performed using an idealized thermal scenario consisting of heating a specimen containing 150 ppm of hydrogen up to 400 °C, ensuring complete dissolution of pre-existing hydrides, followed by a short holding period and subsequent cooling to room temperature. The cooling rate was varied over five orders of magnitude in order to systematically assess the model response to transient thermal conditions.

The simulation results obtained with both models for the mean hydride length and the total volumetric density of hydrides $(N_r + N_t)$ are presented in Fig. 4. It can be observed that the updated model exhibits a significantly reduced sensitivity to the cooling rate and, in addition, produces a much smoother dependence of both quantities on this parameter. This behavior is a key factor contributing to the improved agreement with the SPIZWURZ experimental data discussed above. The original model demonstrates a non-smooth, piecewise-like dependence, characterized by abrupt changes in the predicted quantities. This behavior can be attributed to the occurrence of successive nucleation waves at lower temperatures. Experimental measurements of hydride density and mean length over a broad range of cooling rates would provide a direct validation of the predicted dependencies shown in Fig. 4.

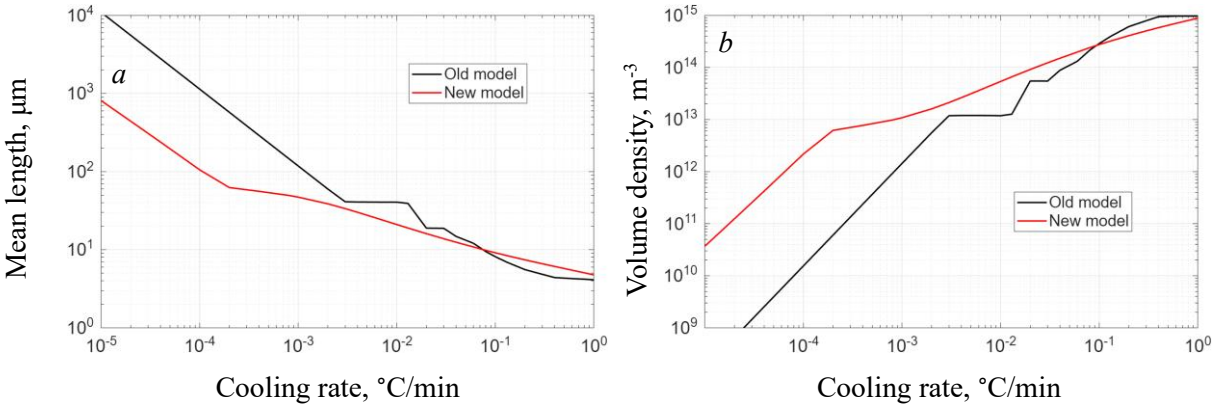


Figure 4. Comparison of two models. The results of simulation a test with linear cooling with differnet cooling rates

In this sense, the classical CNT-based formulation can be interpreted as a local-response model driven by instantaneous thermodynamic conditions, which may lead to nucleation being triggered by transient

fluctuations rather than physically meaningful conditions. The proposed model overcomes this limitation by introducing a time-integrated nucleation criterion.

Figure 5 presents an additional comparison of the simulated hydride morphology with experimental data for rod 4 from the SPIZWURZ test [21]. Rod 4 was very similar to rod 8 discussed above: both rods were fabricated from Zircaloy-4 cladding tubes, hydrogenated to a target concentration of 100 ppm, and positioned symmetrically in the test bundle, which resulted in nearly identical temperature histories. The only difference was the internal gas pressure, equal to 104 bar for rod 4 and 146 bar for rod 8.

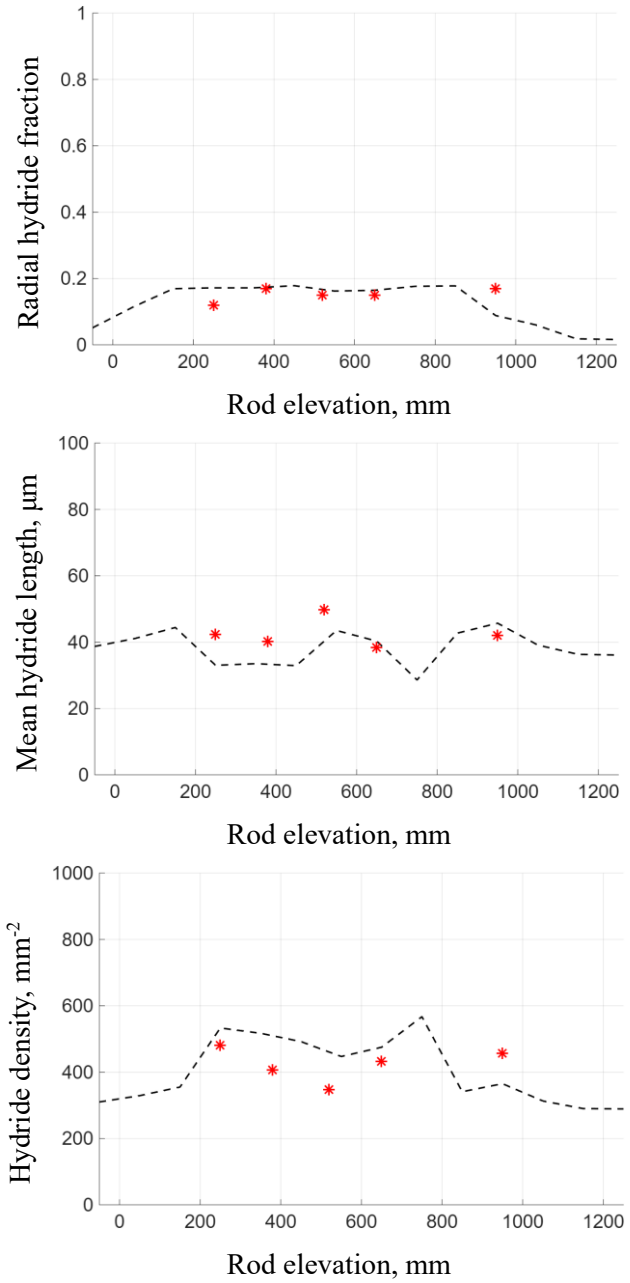


Figure 5. Simulation-to-experiment comparison for rod 4 from the SPIZWURZ test: markers denote experimental data, and lines denote simulation results

5. CONCLUSIONS

The hydride nucleation model based on classical heterogeneous one-step nucleation theory was shown to exhibit an unphysically high sensitivity to variations in hydrogen concentration in the sample, contradicting to experimental data. Small changes in hydrogen content or thermal history resulted in disproportionately large variations in predicted hydride characteristics, limiting the applicability of the original formulation for realistic dry storage conditions.

To overcome these limitations, the model was extended by incorporating a two-stage nucleation mechanism, in which stable δ-hydrides form through intermediate metastable states, along with an explicit treatment of the incubation time required for their transformation into stable nuclei. This formulation combines a reduced nucleation barrier associated with metastable precursor phases and an explicit incubation time representing diffusion-controlled transformation kinetics. This approach introduces a physically justified delay between favorable thermodynamic conditions and the formation of stable hydrides.

The updated model improves robustness by introducing a history-dependent nucleation criterion, reducing sensitivity to cooling rate, and resulting in significantly better agreement with experimental data. Although some discrepancy in variability remains, the overall agreement is considered satisfactory. The proposed approach provides a more physically consistent framework for modeling hydride nucleation under dry storage conditions.

REFERENCES

[1] M. P. Puls, *The Effect of Hydrogen and Hydrides on the Integrity of Zirconium Alloy Components*. London: Springer-Verlag, 2012.

[2] A. T. Motta *et al.*, "Hydrogen in zirconium alloys: A review," *J. Nucl. Mater.*, 518 (2019) 440–460; DOI: 10.1016/j.jnucmat.2019.02.042.

[3] M. Kolesnik, "Micro-mechanisms of the ductile-to-brittle transition in hydrogenated zirconium alloys: A review and a comparison analysis of experimental data and theoretical approaches," *Eng. Fail. Anal.*, 159 (2024) 108110; DOI: 10.1016/j.engfailanal.2024.108110.

[4] X. Wang *et al.*, "Effect of Process Variables on Texture and Hydride Orientation of Cold Pilgered Zr-Sn-Nb-Fe Cladding Tubes," *J. Mater. Eng. Perform.*, 2023, DOI: 10.1007/s11665-023-09006-w.

[5] D. Hardie and M. W. Shanahan, "Stress reorientation of hydrides in zirconium-2.5% niobium," *J. Nucl. Mater.*, 55 (1975) 1–13, DOI: 10.1016/0022-3115(75)90132-4.

[6] Z. Zhao *et al.*, "Identification and characterization of a new zirconium hydride," *J. Microsc.*, 232 (2008) 410–421, DOI: 10.1111/j.1365-2818.2008.02136.x.

[7] N. N. Badr *et al.*, "On the stable/metastable nature of the γ-hydride phase in Zircaloy-2: Microstructural characterization by electron diffraction, electron energy-loss spectroscopy, and diffraction line profile analysis," *J. Nucl. Mater.*, 595 (2024). DOI: 10.1016/j.jnucmat.2024.155058.

[8] G. Yuan, G. Cao, Q. Yue, L. Yang, J. Hu, and G. Shao, "Formation of nanocrystalline δ-ZrHx in Zircoloy-4: Orientation relationship and twinning," *J. Alloys Compd.*, 658 (2016) 494–499; DOI: 10.1016/j.jallcom.2015.10.256.

[9] T. Maimaitiyili *et al.*, "Observation of the δ to ε Zr-hydride transition by in-situ synchrotron X-ray diffraction," *Cryst. Res. Technol.*, 51 (2016) 663–670; DOI: 10.1002/crat.201600234.

[10] N. N. Badr *et al.*, "On Interfacial Ribbons of ζ- and γ-Hydride Phases Surrounding δ Precipitates in Zircaloy-2," *Zircon. Nucl. Ind. 20th Int. Symp.*, 2023, 695–722; DOI: 10.1520/stp164520220058.

[11] X. Zhu, D. Y. Lin, J. Fang, X. Y. Gao, Y. F. Zhao, and H. F. Song, "Structure and thermodynamic

properties of zirconium hydrides by structure search method and first principles calculations," *Comput. Mater. Sci.*, 150 (2018) 77–85; DOI: 10.1016/j.commatsci.2018.03.066.

[12] M. Christensen *et al.*, "H in -Zr and in zirconium hydrides: Solubility, effect on dimensional changes, and the role of defects," *J. Phys. Condens. Matter*, 27 (2025) 2; DOI: 10.1088/0953-8984/27/2/025402.

[13] I. C. Njifon and E. Torres, "A first principles investigation of the hydrogen-strain synergy on the formation and phase transition of hydrides in zirconium," *Acta Mater.*, 202 (2021) 222–231; DOI: 10.1016/j.actamat.2020.10.030.

[14] G. J. C. Carpenter and J. F. Watters, "An in-situ study of the dissolution of γ-zirconium hydride in zirconium," *J. Nucl. Mater.*, 73 (1978) 190–197; DOI: 10.1016/0022-3115(78)90559-7.

[15] S. M. Liu, A. Ishii, S. B. Mi, S. Ogata, J. Li, and W. Z. Han, "Dislocation-Mediated Hydride Precipitation in Zirconium," *Small*, 18 (2022) 1–8; DOI: 10.1002/smll.202105881.

[16] J. Li, Z. Wang, H. Wu, and G. Chen, "Microstructural and crystallographic analysis of hydride reorientation in a zirconium alloy cladding tube," *J. Nucl. Mater.*, 537 (2020) 152232; DOI: 10.1016/j.jnucmat.2020.152232.

[17] S. Liang *et al.*, "Hydride precipitation dependence on α-parent orientation and plastic deformation in zirconium alloys," *Acta Mater.*, 259 (2023) 119292; DOI: 10.1016/j.actamat.2023.119292.

[18] Q. Fang, M. R. Daymond, and A. King, "Study on the morphology of bulk hydrides by synchrotron X-ray tomography," *Mater. Charact.*, 134 (2017) 362–369; DOI: 10.1016/j.matchar.2017.11.013.

[19] M. Kolesnik, T. Aliev, and V. Likhanskii, "Modeling of size, aspect ratio, and orientation of flattened precipitates in the context of Zr-H system under external stress," *Comput. Mater. Sci.*, 189 (2021) 110260; DOI: 10.1016/j.commatsci.2020.110260.

[20] M. Grosse *et al.*, "The SPIZWURZ project – Experimental investigations and modeling of the behavior of hydrogen in zirconium alloys under long-term dry storage conditions," *Nucl. Eng. Technol.*, 56 (2024) 824–831; DOI: 10.1016/j.net.2023.09.027.

[21] M. Kolesnik, J. Stuckert, M. Grosse, and S. Weick, "Hydride morphology in zirconium cladding tubes after the SPIZWURZ bundle test . Part I : analysis of experimental data," *J. Nucl. Mater.*, 619 (2026) 156250; DOI: 10.1016/j.jnucmat.2025.156250.

[22] A. R. Massih and L. O. Jernkvist, "Stress orientation of second-phase in alloys: Hydrides in zirconium alloys," *Comput. Mater. Sci.*, 46 (2009) 1091–1097; DOI: 10.1016/j.commatsci.2009.05.025.

[23] J. Bair, M. Asle Zaeem, and D. Schwen, "Formation path of δ hydrides in zirconium by multiphase field modeling," *Acta Mater.*, 123 (2017) 235–244; DOI: 10.1016/j.actamat.2016.10.056.

[24] H. I. Aaronson, M. Enomoto, and J. K. Lee, *Mechanisms of Diffusion Phase Transformations in Metals and Alloys*. CRC Press, 2010.

APPENDIX A

Table I. Key model parameters used in the simulations

Parameter	Value or correlation
$\gamma' = \gamma_n - \gamma_{gr} \cdot S_{cs}/S_n$	lognormally distributed variable in J/m^2: $\mu = -2.706$, $\sigma = 0.935$
$n_{\max}$	$2 \cdot 10^{15}$ m^{-3}
τ_{dec}	$10^{-9} \cdot \exp(1[\text{eV}]/kT)$ s
L_{eff}	$5 \cdot 10^{-6}$ m
$\Delta\Omega$	$4.93 \cdot 10^{-28}$ m^3
f_0	700